Steel and Composite Structures, *Vol. 31, No. 5* (*2019*) *517-527*
DOI: https://doi.org/10.12989/scs.2019.31.5.517

Ozonization of SWCNTs on thermal/mechanical properties of basalt fiber-reinforced composites

Seong Hwang Kim, Young-Jung Heo and Soo-Jin Park*

Department of Chemistry, *Inha University*, *100 Inharo*, *Incheon 22212*, *South Korea*

(*Received January 2, 2019, Revised April 5, 2019, Accepted April 13, 2019*)

Abstract. To move forward in large steps rather than in small increments, the community would benefit from a systematic and comprehensive database of multi-scale composites and measured properties, driven by comprehensive studies with a full range of types of fiber-reinforced polymers. The multi-scale hierarchy is a promising chemical approach that provides superior performance in synergistically integrated microstructured fibers and nanostructured materials in composite applications. Achieving high-efficiency thermal conductivity and mechanical properties with a simple surface treatment on single-walled carbon nanotubes (SWCNTs) is important for multi-scale composites. The main purpose of the project is to introduce ozone-treated SWCNTs between an epoxy matrix and basalt fibers to improve mechanical properties and thermal conductivity by enhancing dispersion and interfacial adhesion. The obvious advantage of this approach is that it is much more effective than the conventional approach at improving the thermal conductivity and mechanical properties of materials under an equivalent load, and shows particularly significant improvement for high loads. Such an effort could accelerate the conversion of multi-scale composites into high performance materials and provide more rational guidance and fundamental understanding towards realizing the theoretical limits of thermal and mechanical properties.

Keywords: fiber reinforced polymers (FRP); fracture/fracture criteria; hybrid structures; shear-lag effect; bending and shear strength

1. Introduction

Over the years, the use of fiber-reinforced polymer composites (FRPs) has increased in aerospace applications, sports, automotive parts, ocean equipments, and electronic industries because these composites exhibit excellent mechanical properties (Ko *et al*. 2003, Ajayan and Tour 2017, Kolahdouzan *et al*. 2018). FRPs have generally been reinforced with carbon, glass, acrylic, and aramid fibers, allowing conditions that exclude metal use and successfully replacing existing building materials (Shishevan *et al*. 2017, Chen *et al*. 2009). However, with research activities now focused on a green environment, the threat of global warming, and the environmental regulations of various countries, researchers realize the need for eco-friendly fibers (Zhang *et al*. 2012, Carmisciano *et al*. 2011). Therefore, the researchers have suggested the use of eco-friendly, basalt fiber-reinforced polymer composites (BFRPs) as an effective solution to the concerns addressed above (Kim *et al*. 2018).

Basalt rocks are abundant and account for 33% of the earth’s crust, and are very exquisitely divided into small particles and manufacture into a form of fibers (Dhand *et al*. 2015). Basalt fibers (BFs) are highly economical and have an advantage in mass production over other fibers and have an excellent modulus, strength, corrosion resistance, heat resistance and chemical resistance in comparison with glass fibers (Quagliarini *et al*. 2012, Sarasini *et al*. 2013, Czigany *et al*. 2005). From these benefits, BFRPs are emerging as a good alternative to glass FRPs. However, due to drawbacks such as structural defects and inert surfaces, BFs exhibit low interfacial adhesion and thermal conductivity inside the polymer matrix and exhibit lower performance than carbon and aramid fibers (Zhang *et al*. 2012, Lee *et al*. 2015, Deak *et al*. 2010). Therefore, the interfacial adhesion problem of BFRPs has intensified research on advanced interfacial interactions, and prompted fundamental studies to develop composites with improved thermal conductivity and mechanical properties (Ozturk *et al*. 2007, Mittal and Rhee 2018).

Single-walled carbon nanotubes (SWCNTs) have frequently been considered as a multi-scale nano-reinforcement material within a polymer matrix due to their excellent mechanical and physical properties (Tahouneh 2018, Ajayan *et al*. 2000, Wong *et al*. 1997). Recent research by many professionals has reported that multi-scale composites with both nano-scale CNTs and micro-scale fibers within a polymer matrix possess better mechanical properties than conventional FRPs (Shokravi 2017, Ahmadi *et al*. 2016). Multi-scale composites made of SWCNTs provide the possibility to transfer their excellent properties of the nano-scale to the micro-scale. However, SWCNTs are inherently hydrophobic materials, and because of their high aspect ratio, they aggregate and have difficulties associated with poor interfacial interactions

---

*Corresponding author, Professor,
E-mail: sjpark@inha.ac.kr

http://www.techno-press.org/?journal=scs&subpage=6

ISSN: 1229-9367 (Print), 1598-6233 (Online)

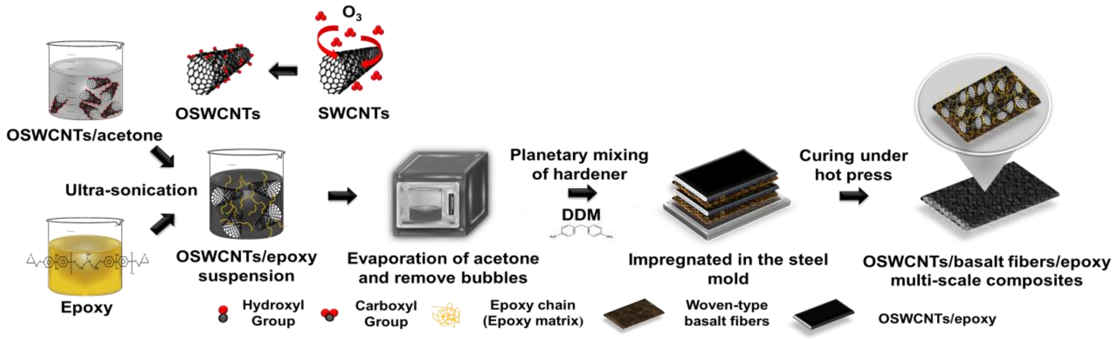

Fig. 1 Schematic representation of OSWCNTs/BFs/epoxy multi-scale composites preparation process

within the polymer matrixes (Kwon *et al*. 2017, Ma *et al*. 2010, Moradi-Dastjerdi and Payganeh 2017). For the success of multi-scale composites reinforced by SWCNTs, excellent dispersion and interfacial adhesion between the SWCNTs and the polymer matrix must be guaranteed. Thus, research has been conducted on ozone treatment to improve the dispersion of SWCNTs in the polymer matrix and to promote their interaction with polymer resins (Tang *et al*. 2011, Sham and Kim 2006, Xu *et al*. 2014, Lee *et al*. 2013). Ozone treatment is an environmentally friendly and is a simple process compared with other surface modification processes. This method can also be performed in an air atmosphere and can improve interfacial interactions and dispersibility by inducing the oxygen-containing functional groups of SWCNTs (Lee *et al*. 2013, Najafi *et al*. 2006). SWCNTs attach various oxygen functional groups, such as -OH, -C = O, and -COOH, to their surface through ozone treatment, which is a dry oxidation method, that improve interfacial adhesion within the matrix (Byl *et al*. 2005). In this respect, Tang *et al*. (2011) modified the surface of CNTs using ozone and found that it strengthened the interface and improved the mechanical properties of epoxy composites. Sham and Kim (2006) demonstrated that ozone treatment can enhance the dispersion of CNTs in the epoxy and accelerate the chemical reaction with the epoxy resin. Therefore, ozone treatment of SWCNTs improves interfacial adhesion within an epoxy matrix for fabricating composites. Nevertheless, there are no studies devoted to research on BF-reinforced epoxy composites with ozone-treated SWCNTs. The functional groups on the surface of ozone-treated SWCNTs improve dispersion and interfacial interactions, and as a result, may produce a greater synergistic effect on the thermal conductivity and mechanical properties of multi-scale composites.

In this study, we propose a method for an efficient and accurate evaluation of the thermal conductivity and mechanical performance of multi-scale composites. The chemical and morphological changes of ozone-treated SWCNTs are investigated, and we prepare specimens with different contents of SWCNTs to compare the synergistic effects of the fabricated multi-scale composites.

2. Experimental

2.1 Materials

The BFs used in this study were commercial, woven-type BFs (EcoB4-F260, Secotech Co, Korea) with an area density of 260 g/m^2. The epoxy resin was diglycidyl ether bisphenol-A (DGEBA) (YD-128, Kukdo Chemical Co, Korea), and 4,4’-diaminodiphenylmethane (DDM), (Sigma-Aldrich Co, Korea) was used as curing agent. In addition, SWCNTs (Ocsial Co, Korea) with a diameter of 1.6 ± 0.3 nm were used.

2.2 Ozone treatment of SWCNTs

The ozone-treated SWCNTs were prepared using the following procedure. The ozone treatment was performed using an ozone generator (Ozonizer, Ozone Tech Co, Lab II, Korea) as a dry oxidation method, and generator parameters were set to 220 V and 60 Hz to generate ozone from oxygen gas. Ozone was produced at 8 g/h under 0.08 MPa with an O_3 gas flow of 0.8 l/min, and the SWCNTs ozone treatment was carried out at room temperature for 2 h. The ozone-treated SWCNTs were denoted as OSWCNTs.

2.3 Fabrication of OSWCNTs/BFs/epoxy multi-scale composites

Fig. 1 illustrates the OSWCNTs/BFs/epoxy multi-scale composite preparation process. OSWCNT/BFs/epoxy multi-scale composites were prepared using the following procedure: First, OSWCNTs (0.1, 0.3, 0.5, and 0.7 wt%) were dissolved in acetone, and then ultrasonicated for 30 min before being suspended in epoxy resin. Then, the mixed OSWCNTs/epoxy was heated in a vacuum oven at 115°C for 1 h to evaporate the acetone and remove bubbles. Thereafter, the OSWCNTs/epoxy and hardener (DDM) were mixed together in a planetary mixer for 5 min. Following this, the laminates were prepared by continuous impregnation of the BFs using a 3-roll-mill machine for manufacturing unidirectional prepregs with subsequent hot pressing (Yim *et al*. 2015). Finally, the laminated plate was hot-pressed (3 MPa, 180°C, 150 min), thereby yielding the final specimen. We denoted the specimens of SWCNTs/ BFs/epoxy multi-scale composites and OSWCNTs/BFs/

Table 1 Composition of SBE and OSBE multi-scale composites

Specimens	Epoxy resin (wt %)	Basalt fibers (wt %)	SWCNTs (wt %)	OSWCNTs (wt %)
Neat	100	50	-	-
SBE-1	100	50	0.1	-
SBE-2	100	50	0.3	-
SBE-3	100	50	0.5	-
SBE-4	100	50	0.7	-
OSBE-1	100	50	-	0.1
OSBE-2	100	50	-	0.3
OSBE-3	100	50	-	0.5
OSBE-4	100	50	-	0.7

epoxy multi-scale composites as SBE and OSBE, respectively. Details of the multi-scale composite specimens are shown in Table 1.

2.4 Characterization of OSBE multi-scale composites

The surface properties of the OSWCNTs were investigated using a Fourier transform-infrared vacuum spectrometer (FT-IR) (Bruker Optik Co, Vertex 80V, USA), X-ray photoelectron spectrometer (XPS) (Thermo Scientific Co, K-Alpha, USA), and Raman microscope (Raman) (Bruker Optics Co, Senterra R200-L, Germany). The surface morphologies of the prepared OSWCNTs and multi-scale composites were investigated using high-resolution scanning electron microscopy (HR-SEM) (Hitachi Technologies Co, SU8010, Japen) and field-emission transmission electron microscopy (FE-TEM) (Jeol Co, JEM-2100F, USA).

2.5 testing of OSBE multi-scale composites

The thermal conductivity of the multi-scale composites was determined in a thermal conductivity analyzer (Laser flash, Netzsch Co, LFA-447, Germany). Before the measurement, both sides of the composites were coated with graphite spray. The thermal conductivity could be calculated using the following Eqs. (1)-(2) (Choi and Park 2013)

$$\kappa = \alpha\, \rho\, Cp \tag{1}$$

In Eq. (1), κ is the thermal conductivity of the specimen, α and ρ are the thermal diffusivity and the density of the specimen, and Cp is the specific heat of the specimen. The specific heat was tested by DSC, the density tested by a density gauge, and the thermal diffusivity obtained by Eq. (2)

$$\alpha = \frac{1.38Y^2}{\pi^2 t_{1/2}} \tag{2}$$

Table 2 Surface energy, specific of the test wetting liquids used

Wetting liquids	γL (mJ·m^{-2})	γ_L^L (mJ·m^{-2})	γ_L^{SP} (mJ·m^{-2})
Diiodomethane	50.80	50.42	0.38
Ethylene glycol	47.70	31.00	16.70
Distilled water	72.80	21.80	51.00

In Eq. (2), Y is the thickness of the specimen and t is the time. The specimens of the tested multi-scale composites were observed for thermal absorption and dissipation capability using an infrared thermal camera.

Dynamic contact angle was measured using the sessile drop method on a Rame-Hart goniometer (SEO Co,Phoenix 300 Plus, Korea). The wetting liquids used in the contact angle measurement were diiodomethane, ethylene glycol, and distilled water. The droplet volume of the standard wetting solution was 5 μL, determined at room temperature (25 ± 1°C) for each liquid. For each specimen, calculated contact angles were obtained at 15 random locations on the multi-scale composite surface, with a standard deviation below 1°. The basic liquid characteristics of surface energy (or surface tension), London dispersion force, and specific polar components are shown in Table 2.

The fracture toughness (K_{IC}) of the multi-scale composites was determined by a 3-point bending test to assess the extent to which the critical stress intensity factor (K_{IC}) was resistant to fracture in accordance with ASTM E-399. K_{IC} determined from the 3-point bending tests was calculated as Eqs. (3)-(4) (Dong *et al*. 2014, Galpaya *et al*. 2014)

$$K_{\mathrm{IC}} = \frac{FL}{bd^{3/2}} \cdot Y \tag{3}$$

In Eq. (3), F(N) is the critical load at crack fracture, L (mm) is the distance between span supports, and b and d (mm) are the width and the thickness of the specimen.

$$Y = \frac{3a/d^{1/2}[1.99-(a/d)(1-a/d)(2.15-3.93a/d+(2.7a^2/d^2)]}{2(1+2a/d)(1-a/d)^{3/2}} \tag{4}$$

In Eq. (4), a (mm) is the pre-crack length. Pre-crack length were cut using a slow-speed diamond wire saw, approximately half the depth of the specimen. The specimens of the tested multi-scale composites were platinum coated, and the fracture planes were observed.

The interlaminar shear strength (ILSS) was determined using short-beam 3-point bending tests to assess the interfacial adhesion strength of the multi-scale composites, in accordance with ASTM D-2344. ILSS determined from short-beam 3-point bending tests was calculated as Eq. (5) (Ryu *et al*. 1999, Ray 2004)

$$ILSS = \frac{0.75F}{bd} \tag{5}$$

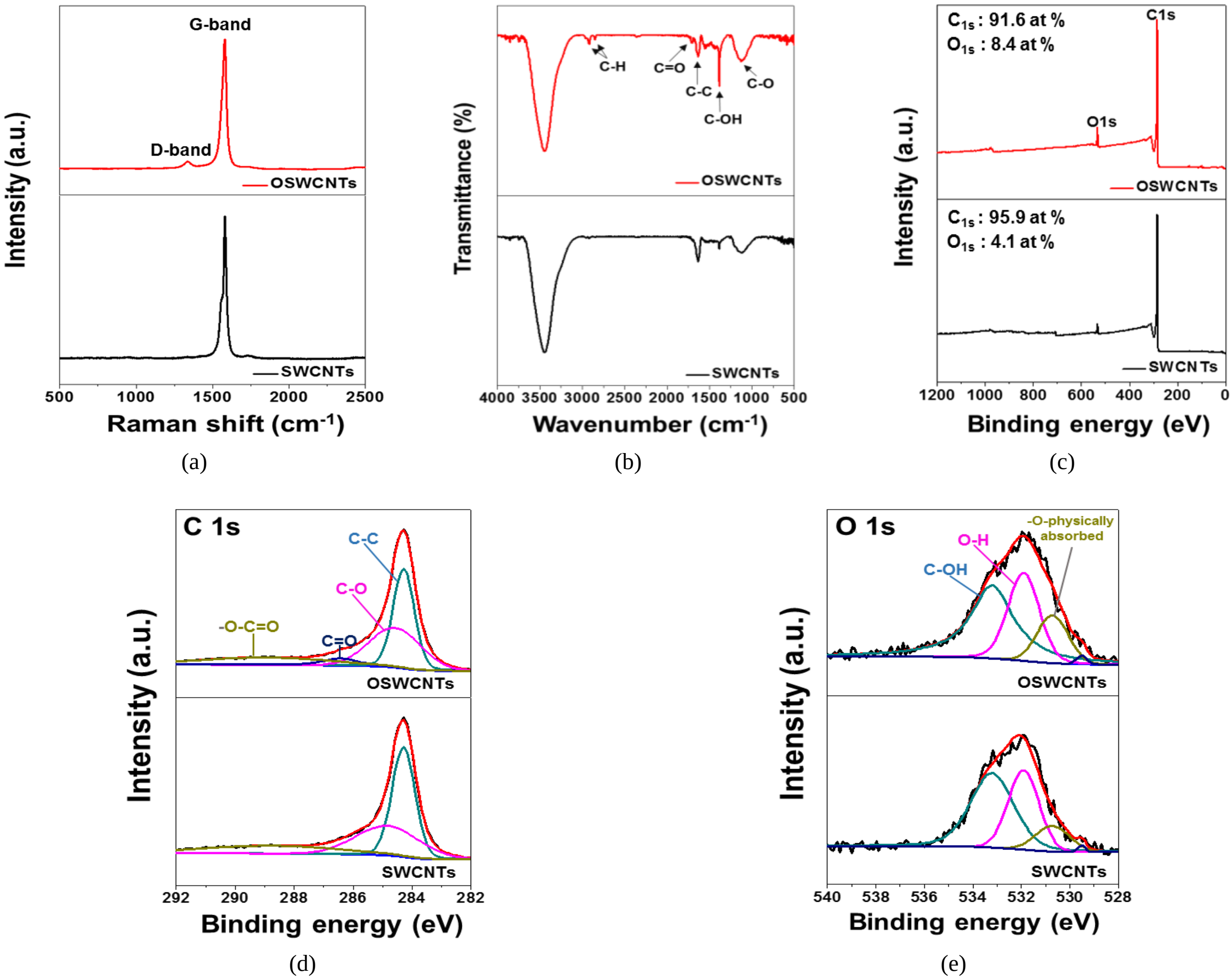

(a) (b) (c)

(d) (e)

Fig. 2 Characterization of SWCNTs and OSWCNTs: (a) Raman spectra, (b) FT-IR spectra, (c) high-resolution XPS spectra, (d) C1s core level of XPS spectra, and (e) O1s core level of XPS spectra

3. Results and discussion

3.1 Characterization of OSWCNTs

From Fig. 2(a), the Raman spectra show the increase in intensity of the D-band associated with the number of defects in the OSWCNTs compared with the SWCNTs. The peaks at 1579.8 cm^{-1} and approximately 1335.7 cm^{-1} correspond to typical G-band (graphite) and D-band (defects in the amorphous nanotube walls) features, and the relative intensities between the two peaks provide information on the quality (Alharbi *et al*. 2018). The D-band of the OSWCNTs was increased by the introduction of oxygen functionalities in some amorphous nanotube sidewalls through continuous dry oxidation during the ozone treatment process.

Fig. 2(b) shows the FT-IR spectra of SWCNTs and OSWCNTs. After ozone treatment for 2 h, new peaks could be observed at 1701.5 and 1128.2 cm^{-1}, which are attributed to the C-O and C = O stretching vibrations of the carboxylic groups (–COOH), respectively (Wang *et al*. 2018). The peaks at 2918.2 and 1384.6 cm^{-1} correspond to the expected C–H and C–OH stretching vibrations, as confirmed by the decrease in the C-C band at 1645.3 cm^{-1}, respectively (Mawhinney *et al*. 2000, Li *et al*. 2007). To confirm further the surface oxygen composition of the OSWCNTs, XPS survey spectra were performed and relative analysis. The XPS survey spectra and subsequently detected atomic concentration of the elements carbon (C) and oxygen (O) at the SWCNTs and OSWCNTs surfaces are presented in Fig. 2(c). The C/O ratio of OSWCNT is reduced by about 115% compared with the received SWCNTs, and it can be demonstrated that oxygen-containing functional groups were introduced on the nanotube surfaces after the ozone treatment.

To support this explanation, we observed high-resolution single-scan spectra of the C1s and O1s core levels in Figs. 2(d) and (e), respectively. Fig. 2(d) shows the C1s deconvolution peaks at 284.2, 284.6, 286.4, and 288.8 eV, corresponding to the C-C, C-O, C=O and -O-C=O groups, respectively (Mishra *et al*. 2016, Sui *et al*. 2018). Fig. 2(e) shows the O1s deconvolution peaks at 530.8, 531.8, and 533.2 eV, corresponding to the physically adsorbed -O, O-H, and C-OH groups, respectively (Datsyuk *et al*. 2008). OSWCNTs are found to have more hydroxyl and carboxylic functionalities on the outer surface compared to the as-received SWCNTs. This implies that the amount of oxygen found in the OSWCNTs promotes the adsorption of oxygen molecules by forming an electron-rich region of amorphous nanotube sidewalls that are removed during the dry oxidation deposition process (Sham and Kim 2006). Therefore, the number of oxygen-containing functional groups was increased by ozone treatment of the SWCNTs, and this is reflected consistently with the above-mentioned Raman and FT-IR data.

3.2 Mophology of OSWCNTs

From Figs. 3(a) and (b), the difference in surface morphology between the SWCNTs and OSWCNTs is observed. Fig. 3(a) shows the SWCNTs have a large aspect ratio with a smooth surface along the axis and exhibit a typical shape with random structure. However, in Fig. 3(b), the OSWCNTs structure shows an important change on their surface morphology. In the functionalization process of SWCNTs, the ozonization was observed to increase the defects/damage on the SWCNTs surface. For a more detailed observation, the magnified TEM image in Figs. 3(c) and (d) shows the surface roughness of the SWCNTs and OSWCNTs. A comparison of Fig. 3(c) with Fig. 3(d) clearly reveals the existence of grooves along the amorphous nanotube sidewalls of the OSWCNTs. This is because ozonization begins at the outer layer and progressively removes some of the amorphous nanotube sidewalls of the SWCNTs through continuous oxidization.

3.3 Thermal conductivity of OSBE multi-scale composites

Nano-reinforcement materials with a high aspect ratio such as SWCNTs have been reported to be able to improve heat transfer because they build a more continuous thermal conductivity network in multi-scale composites (Gojny *et al*. 2006, Li *et al*. 2018). However, dispersing SWCNTs in epoxy matrix systems is a difficult process, and uniform dispersion in epoxy matrix is the most important factor in fabricating multi-scale composites with excellent thermal conductivity in the SWCNTs. Therefore, excellent dispersion and surface properties of OSWCNTs in an epoxy matrix is instructive in build a thermal conductivity network, which is critical to the thermal conductivity of multi-scale composites (Karaipekli *et al*. 2017). The results in Table 3 and Fig. 4 suggest that for OSBE composites, higher thermal conductivity is obtained by forming a better thermal conductivity network than SBE composites. At the initial stage, the OSBE-1 and OSBE-2 composites increased about 3.0 and 6.3% compared to the SBE-1 and SBE-2 composites. Thermal conductivity was not significantly changed until that OSBE-2 composites, but from the OSBE-3 and OSBE-4 composites showed a significant difference. The OSBE-3 composites (0.490 W.mK^{-1}) increased significantly to about 14.2% compared to SBE-3 composites (0.429 W.mK^{-1}). In addition, OSBE-4 composites (0.554 W.mK^{-1}) increased significantly to about 9.3% compared to SBE-4 composites (0.507 W.mK^{-1}).

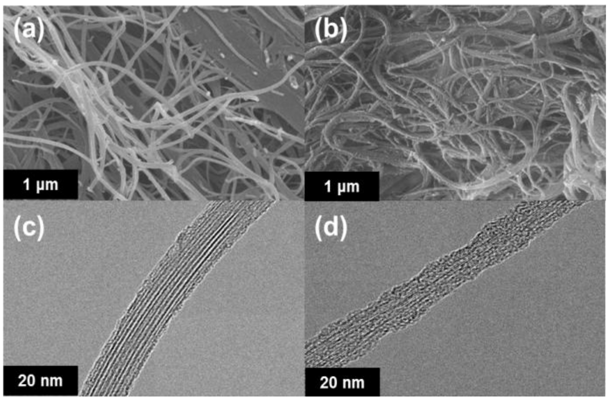

Fig. 3 Surface morphology: (a) and (b) are SEM images of SWCNTs and OSWCNTs, (c) and (d) are high resolution TEM images of SWCNTs and OSWCNTs

We compared heat absorption and dissipation to simulate the real heat transfer capability of SBE and OSBE composites, and the temperature change in the composites under the same heating and cooling conditions were observed by an infrared thermal camera. In the case of the heating process, we measured the temperature change in the composites every 10 s on a hot plate at 120 °C. The temperature change curve for heat absorption over time is shown in Fig. 5(a), and the heat absorption optical image is shown in Fig. 5(c). The temperature of the neat and SBE-3

Table 3 The thermal conductivity parameter of SBE and OSBE multi-scale composites

Specimens	Density (g.cm^{-3})	Diffusivity (mm^2.s^{-2})	Cp (J.gK^{-1})	Thermal conductivity (W.mK^{-1})
Neat	1.152	0.168±0.001	1.301±0.024	0.252
SBE-1	1.513	0.178±0.001	1.089±0.019	0.293
SBE-2	1.541	0.191±0.001	1.189±0.037	0.350
SBE-3	1.584	0.211±0.001	1.283±0.009	0.429
SBE-4	1.612	0.232±0.001	1.356±0.016	0.507
OSBE-1	1.521	0.181±0.001	1.095±0.016	0.302
OSBE-2	1.539	0.203±0.001	1.191±0.023	0.372
OSBE-3	1.582	0.225±0.001	1.377±0.017	0.490
OSBE-4	1.619	0.245±0.001	1.396±0.005	0.554

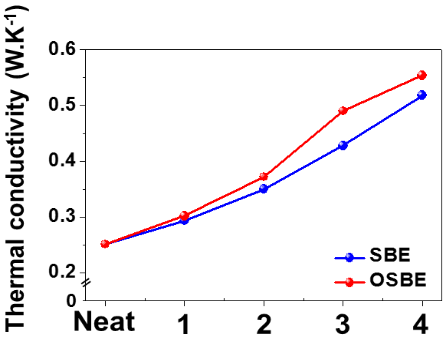

Fig. 4 Thermal conductivity of SBE and OSBE multi-scale composites

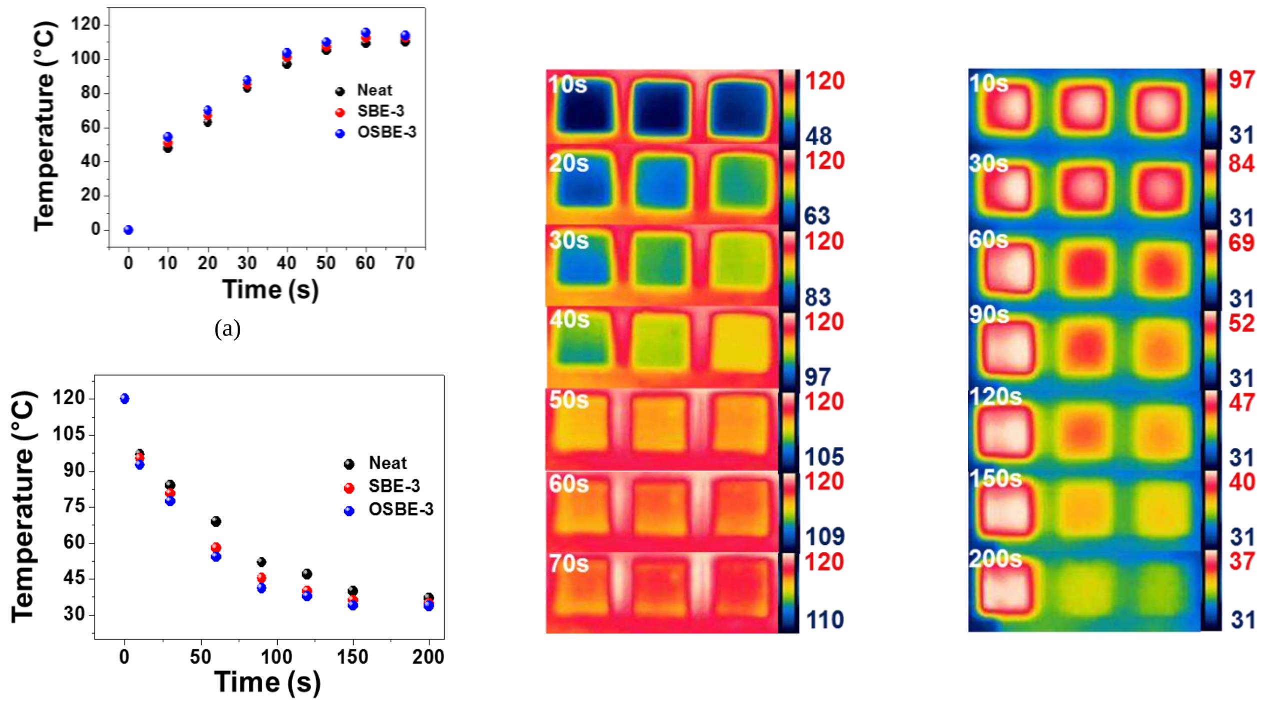

(a) (b) (c) (d)

Fig. 5 Infrared thermal camera of SBE and OSBE multi-scale composites: (a) temperature change curve of heat absorption over time, (b) temperature change curve of heat dissipation over time, (c) optical images of the heat absorption over time, (d) optical images of the heat dissipation over time.

composites changes gradually with heating time, but the OSBE-3 composites show the fastest color change and the highest thermal conductivity. The cooling process was performed by first heating the composites to 120℃ for 2 h in an oven to ensure uniform temperature distribution. Compared with the neat and SBE-3 composites, the OSBE-3 composites exhibited fast heat dissipation (Figs. 5(b) and (d)), indicating high heat transfer capability.

To reveal the effect of OSWCNTs on the thermal conductivity of multi-scale composites, FE-TEM was used to observe the dispersion of OSWCNTs within the matrixes. Figs. 6(a) and (c) shows that the high van der Walls interactions within the epoxy matrix of the SBE-3 composites resulted in spaces. As the thermal conductivity is determined by the number of conductive paths and networks formed in the epoxy matrix, the many void spaces created within the matrix of the SBE-3 composites interfere with building the thermal conductivity network. On the other hand, Figs. 6(b) and (d) how homogeneous dispersion without aggregates within the epoxy matrix of the OSBE-3 composites. This suggests that the strong matrix interactions between epoxy and OSWCNTs is effective in improving thermal conductivity at the same nano-reinforcement material loading, because unnecessary phonon scattering can be voided.

3.4 Interfacial properties of OSBE multi-scale composites

To confirm the interfacial interactions between the OSWCNTs-epoxy matrix and BFs, manufactured multi-scale composite surface energies were measured with a ontact angle. The surface energy value is the degree of interfacial adhesion between the filler–polymer matrix and the fibers, which is important for evaluating the physical interfacial interactions and mechanical properties of multi-scale composites. The surface energy value is calculated based on the contact angle between liquid and solid to obtain accurate surface energy information. In accordance with the method proposed by Fowkes (1962), Owens and Wendt (1969), Kaelble (1970), surface energy is divided into two components

$$\gamma = \gamma^L + \gamma^{SP} \tag{6}$$

$$\gamma_L(1+\cos\theta) = 2\left(\sqrt{\gamma_S^L \cdot \gamma_L^L} + \sqrt{\gamma_S^{sp} \cdot \gamma_L^{sp}}\right) \tag{7}$$

In Eq. (6), γ is the surface energy, γ^L is the dispersion component of the surface energy associated with the Lifshitz-van der Waals interactions that include London forces. γ^{SP} is the specific polar components of the surface energy associated with Keesom's orientational force, hydrogen bonding, and Debye-inductive polarization (dipole-dipole, dipole-induced dipole). In Eq. (7), θ is the contact angle of the liquid droplet, subscript L represents a liquid, and S represents a solid. Using three test liquids with Eqs. (6)-(7), one can accurately determine the surface energy with the following equation (Kaelble 1970)

$$\frac{\gamma_L(1+\cos\theta)}{2\sqrt{\gamma_L^L}} = \sqrt{\gamma_S^{sp}}\left(\frac{\sqrt{\gamma_L^{sp}}}{\sqrt{\gamma_L^L}}\right) + \sqrt{\gamma_S^L}\,. \tag{8}$$

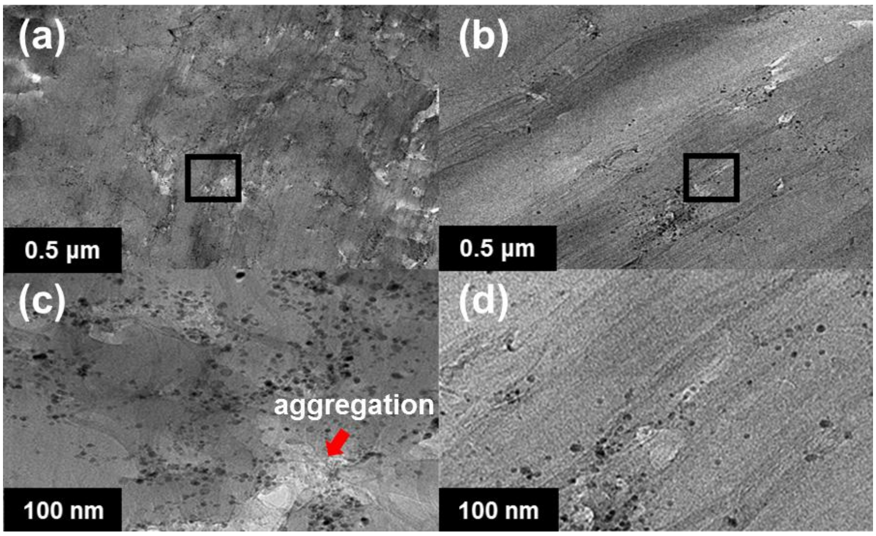

Fig. 6 Surface morphology of SBE and OSBE multi-scale composites: (a) TEM images of SBE-3 composites; (b) TEM images of OSBE-3 composites. (c), (d) magnify TEM images of closed regions in (a), (b), respectively

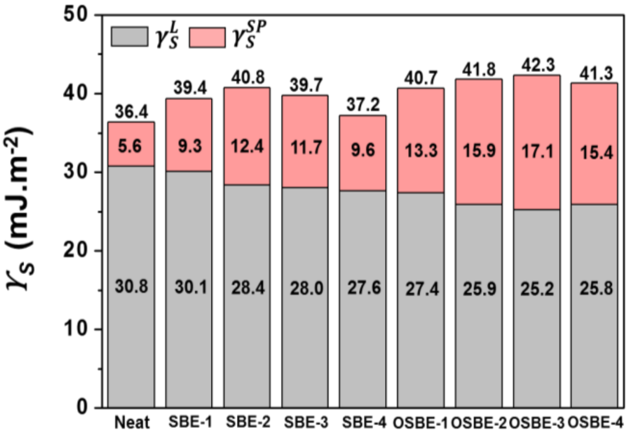

Fig. 7 Surface energy of SEBE and OSBE multi-scale composites on interfacial properties

The surface energy results for the SBE and OSBE multi-scale composites calculated from Eq. (8) are show in Fig. 7. The surface energy of OSBE composites shows an obvious improvement in comparison with that of SBE composites. In Fig. 7, the specific polar component (γ^{SP}) of the OSBE composites has a greater influence on surface energy than the dispersive components (γ^{L}), and the increase in the total surface energy was observed for the specific polar component of the OSBE composites. The interfacial interactions of multi-scale composites were significant not only for the properties of the epoxy matrix and BFs, but also for the effect of the matrix interactions between the epoxy resin and OSWCNTs. To put it concretely, this signifies that specific polar components can be provided because the chemical affinity of the OSWCNTs changes from hydrophobic to hydrophilic due to the various oxygen functional groups (hydroxyl and carboxylic functionalities) introduced. Various polar groups of OSWCNTs have been enhanced with compatible interactions for affinity between the epoxy groups.

To support this explanation, the wetting behavior experiments with SBE-3 and OSBE-3 composites were carried out at 25℃ for 10 min. It can be seen from Fig. 8 that the contact angle of neat composites indicates low wettability due to the chemically inactive surface of the BFs and is maintained at approximately 71.5°. In addition, the contact angle of the SBE-3 composites shows no obvious changes and is maintained near 59°, but the contact angle of the OSBE-3 composites decreased very rapidly and saturated at around 27.4°. This observation signifies excellent tunability of the hydrophobic–hydrophilic interfacial interactions enabled by the OSWCNTs, and this discovery is very meaningful and quite important.

3.5 Mechanical properties of OSBE multi-scale composites

The ILSS is a critical indicator of the interfacial adhesion between the OSWCNT–epoxy matrix and BFs and reveals shear properties that depend on interfacial interactions in the matrix (Bellahcene and Aberkane 2017, Ray (2006), Shi *et al*. 2018). From Fig. 9, it is clearly shown that the linear relationship between the specific polar components of surface energy and the ILSS can improve interfacial adhesion of the multi-scale composites. As a result of this evaluation, the ILSS value of the neat composites (25.7 MPa) showed poor interfacial adhesion as expected, and the SBE composites performed better than the neat composites, but there was still a limit to their interfacial effects. Alternatively, the OSBE composites showed a synergistic effect on interfacial adhesion as compared with the SBE composites. Compared to the SBE-1 (30.3 MPa) and SBE-2 (36.1 MPa) composites, ILSS values of for the OSBE-1 (32.6 MPa) and OSBE-2 (38.5 MPa) composites increased by 7.6% and 6.7%, respectively. In particular, the OSBE-3 (41.4 MPa) and OSBE-4 (36.3 MPa) composites showed a significant increase of 31.9% and 32.5%, respectively, compared with the SBE-3 (31.4 MPa) and SBE-4 (27.4 MPa) composites. This means that

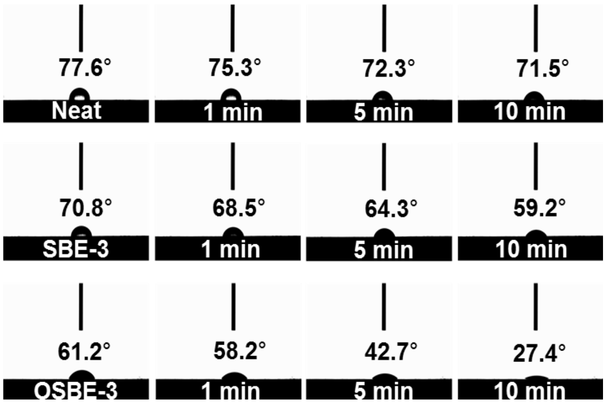

Fig. 8 Optical images of the contact angle of water over time

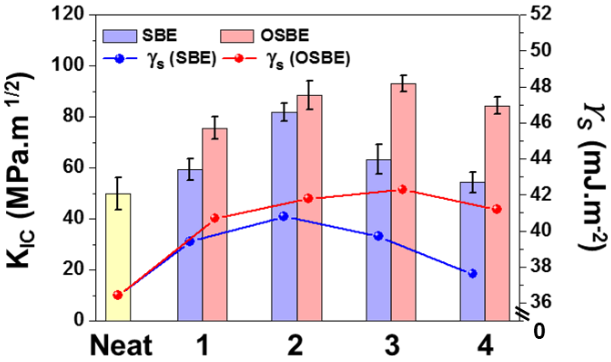

Fig. 10 Correlation between K_{IC} and surface energy in the mechanical properties of SBE and OSBE multi-scale composites

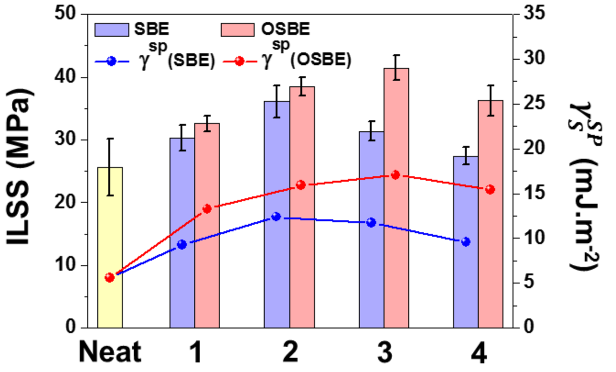

Fig. 9 Correlation between ILSS and specific polar components of surface energy in the interfacial properties of SBE and OSBE multi-scale composites

OSWCNTs are effectively propagated within the epoxy matrix to BFs through simple and effective functionalization even at high loads. Therefore, we suggest that the interactions of OSWCNTs within the epoxy matrix exerts a considerable synergistic effect for improving interfacial adhesion.

Generally, the main ability of SWCNTs as a reinforcing element in an epoxy matrix is known to improve fracture toughness, and is an essential design factor, especially for multi-scale composites intended for application in the structural industry (Eskizeybek *et al*. 2014, Liu and Wilkinson 2018, Ravindran *et al*. 2018). However, as the load of SWCNTs increases, due to incompatible interactions within the epoxy matrix, low dispersibility and interfacial adhesion decreases fracture mechanics in multi-scale composites. Therefore, the improvement of fracture mechanics should effectively support the load of BFs by ensuring not only interfacial adhesion in the composites but also the excellent dispersibility of SWCNTs. Fig. 10 clearly shows that the OSWCNTs of linear behavior between the surface energy and K_{IC} can effectively dispersibility and interfacial adhesion of the multi-scale composites. Compared with the SBE-1 (59.4 MPa.m$^{1/2}$) and SBE-2 (81.9 MPa.m$^{1/2}$) composites, K_{IC} values of OSBE-1 (75.7 MPa.m$^{1/2}$) and OSBE-2 (88.3 MPa.m$^{1/2}$) composites increased by 27.4% and 7.8%, respectively. In addition, OSBE-3 composites (90.7 MPa.m$^{1/2}$) increased significantly to 43.1% compared with SBE-3 composites (63.4 MPa.m$^{1/2}$). Since then, OSBE-4 composites (84.3 MPa.m$^{1/2}$) significantly increased by 55.3% compared with SBE-4 composites (54.3 MPa.m$^{1/2}$) and exhibited similar trends to ILSS. As mentioned above, the addition of OSWCNTs has proved to be an effective way to improve interfacial adhesion of multi-scale composites, even at high loads.

We observed the fracture surfaces in more detail to study the fracture mechanisms acting on the multi-scale composites. Figs. 11(a) and (d) shows a relatively smooth cracked surface of typical brittle fracture mode patterns with regular crack growth in neat composites. These exhibit typical thermosetting polymer properties that are easily broken, and low crack resistance. Figs. 11(b) and (e) shows the SBE-3 composites' very rough crack voids due to non-homogeneous dispersion of SWCNTs, and aggregated fractures were observed due to low interfacial adhesion between the matrix and BFs. These fractures were exhibited at low stress due to the poor interfacial interactions between the SWCNTs and the matrix, which failed to efficiently support the load of the BFs. Fig. 11(f) shows magnified images of the enclosed region in Fig. 11(c), and it was observed that SWCNTs were homogeneously dispersed between the epoxy matrix and BFs. This effectively supports the load of BFs by ensuring dispersibility and interfacial adhesion, and distorts the crack path, making crack propagation difficult. This fracture pattern supports the findings of the highest levels of fracture toughness being associated with dispersibility and interfacial adhesion, as presented in Fig. 11(f).

4. Conclusions

To move forward in large steps rather than in small increments, the community would benefit from a systematic and comprehensive database of multi-scale composites and measured properties, driven by comprehensive studies with a full range of types of FRPs. We focused on the dispersion and interfacial interactions and synergistic effects of ozone-treated SWCNTs in epoxy matrix and BFs and provided a simple approach to increase thermal conductivity and mechanical properties. After ozone functionalization, the

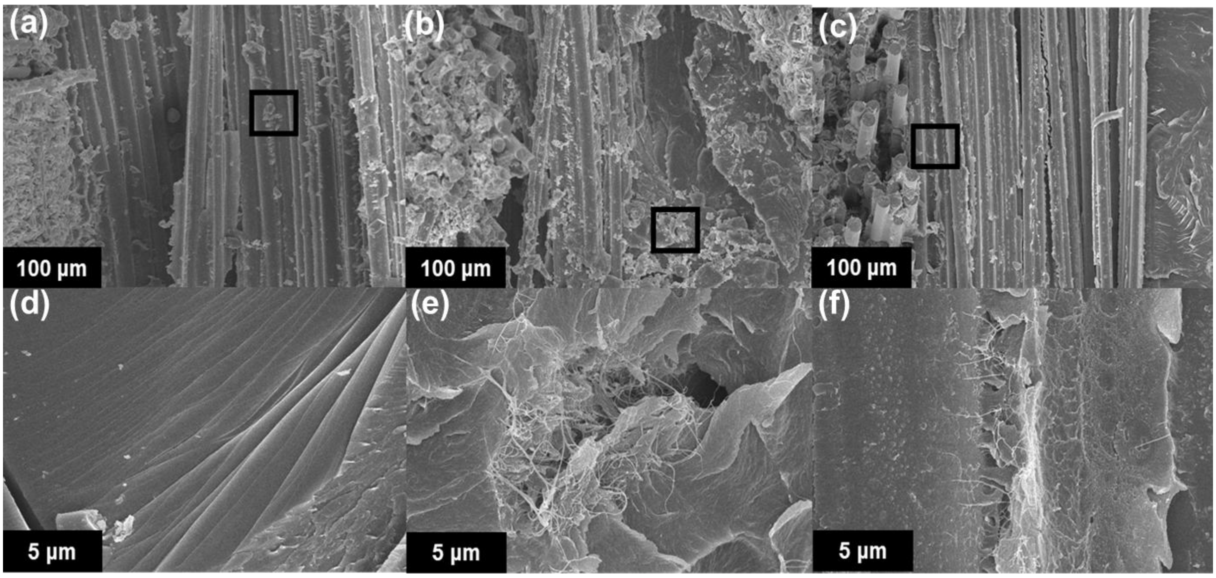

Fig. 11 Surface morphology of SBE and OSBE multi-scale composites: (a) SEM images of SBE-3 composites; (b) SEM images of OSBE-3 composites; (c), (d) magnify SEM images of closed regions in (a), (b), respectively

introduced of hydroxyl and carboxyl functionalities on the SWCNTs surface significantly improved SWCNTs dispersibility and interfacial adhesion due to improved chemical interactions within the epoxy matrix. In addition, ozone-treated SWCNTs were effective in improving thermal conductivity and mechanical properties under the same loading. Such an effort could accelerate the conversion of multi-scale composites into high performance materials and provide more rational guidance and fundamental understanding towards realizing the theoretical limits of thermal and mechanical properties.

Acknowledgments

This work was supported by the Technology Innovation Program (or Industrial Strategic Technology Development Program (10083586, Development of petroleum based graphite fibers with ultra-high thermal conductivity) funded by the Ministry of Trade, Industry & Energy (MOTIE, Korea) and This work was supported by the Technological Innovation R&D Program (S2598148) funded by the Small and Medium Business Administration (SMBA, Korea).

References

Ahmadi, M., Zabihi, O., Masoomi, M. and Naebe, M. (2016), “Synergistic effect of MWCNTs functionalization on interfacial and mechanical properties of multi-scale UHMWPE fibre reinforced epoxy composites”, *Compos. Sci. Technol.*, **134**, 1-11.

Ajayan, P.M. and Tour, J.M. (2007), “Materials science: nanotube composites”, *Nature*, **447**(7148), 1066.

Ajayan, P.M., Schadler, L.S., Giannaris, C. and Rubio, A. (2000), “Single-walled carbon nanotube–polymer composites: strength and weakness”, *Adv. Mater.*, **12**(10), 750-753.

Alharbi, T.M., Vimalanathan, K., Lawrance, W.D. and Raston, C.L. (2018), “Controlled slicing of single walled carbon nanotubes under continuous flow”, *Carbon*, **140**, 428-432.

Bellahcene, T. and Aberkane, M. (2017), “Estimation of fracture toughness of cast steel container from Charpy impact test data”, *Steel Compos. Struct. Int. J.*, **25**(6), 639-648. http://dx.doi.org/10.12989/scs.2017.25.6.639

Byl, O., Liu, J. and Yates, J.T. (2005), “Etching of carbon nanotubes by ozone a surface area study”, *Langmuir.*, **21**(9), 4200-4204.

Carmisciano, S., De Rosa, I.M., Sarasini, F., Tamburrano, A. and Valente, M. (2011), “Basalt woven fiber reinforced vinylester composites: Flexural and electrical properties”, *Mater. Des.*, **32**(1), 337-342.

Chen, W., Shen, H., Auad, M.L., Huang, C. and Nutt, S. (2009), “Basalt fiber–epoxy laminates with functionalized multi-walled carbon nanotubes”, *Compos. Part A Appl. Sci. Manuf.*, **40**(8), 1082-1089.

Choi, J.R. and Park, S.J. (2013), “A study on thermal conductivity and fracture toughness of alumina nanofibers and powders-filled epoxy matrix composites”, *Polym.*, **37**(1), 47-51. [In Korean]

Czigány, T., Vad, J. and Pölöskei, K. (2005), “Basalt fiber as a reinforcement of polymer composites”, *Period. Mech. Eng.*, **49**(1), 3-14.

Datsyuk, V., Kalyva, M., Papagelis, K., Parthenios, J., Tasis, D., Siokou, A. and Galiotis, C. (2008), “Chemical oxidation of multiwalled carbon nanotubes”, *Carbon*, **46**(6), 833-840.

Deák, T., Czigány, T., Tamás, P. and Németh, C. (2010), “Enhancement of interfacial properties of basalt fiber reinforced nylon 6 matrix composites with silane coupling agents”, *Polym. Lett.*, 4(10), 590-598.

Dong, W., Liu, H.C., Park, S.J. and Jin, F.L. (2014), “Fracture toughness improvement of epoxy resins with short carbon fibers”, *J. Industrial. Eng. Chem.*, **20**(4), 1220-1222.

Dhand, V., Mittal, G., Rhee, K.Y., Park, S.J. and Hui, D. (2015), “A short review on basalt fiber reinforced polymer composites”, *Compos. Part B. Eng.*, **73**, 166-180.

Eskizeybek, V., Avci, A. and Gülce, A. (2014), “The Mode I interlaminar fracture toughness of chemically carbon nanotube grafted glass fabric/epoxy multi-scale composite structures”, *Compos. Part A Appl. Sci. Manuf.*, **63**, 94-102.

Fowkes, F.M. (1962), “Determination of interfacial tensions, contact angles, and dispersion forces in surfaces by assuming additivity of intermolecular interactions in surfaces", *J. Phys. Chem.*, **66**(2), 382-382.

Galpaya, D., Wang, M., George, G., Motta, N., Waclawik, E. and Yan, C. (2014), "Preparation of graphene oxide/epoxy nanocomposites with significantly improved mechanical properties", *J. Appl. Phys.*, **116**(5), 053518

Gojny, F.H., Wichmann, M.H., Fiedler, B., Kinloch, I.A., Bauhofer, W., Windle, A.H. and Schulte, K. (2006), "Evaluation and identification of electrical and thermal conduction mechanisms in carbon nanotube/epoxy composites", *Polymer*, **47**(6), 2036-2045.

Karaipekli, A., Biçer, A., Sarı, A. and Tyagi, V.V. (2017), "Thermal characteristics of expanded perlite/paraffin composite phase change material with enhanced thermal conductivity using carbon nanotubes", *Energy Convers. Manag.*, **134**, 373-381.

Kaelble, D.H. (1970), "Dispersion-polar surface tension properties of organic solids", *The J. Adhesion*, **2**(2), 66-81.

Kim, S.H., Heo, Y.J., Park, M., Min, B.G., Rhee, K.Y. and Park, S. J. (2018), "Effect of hydrophilic graphite flake on thermal conductivity and fracture toughness of basalt fibers/epoxy composites", *Compos. Part B. Eng.*, **153**, 9-16.

Ko, F., Gogotsi, Y., Ali, A., Naguib, N., Ye, H., Yang, G.L. and Wilis, P. (2003), "Electrospinning of continuous carbon nanotube-filled nanofiber yarns", *Adv. Mater.*, **15**(14), 1161-1165.

Kolahdouzan, F., Arani, A.G. and Abdollahian, M. (2018), "Buckling and free vibration analysis of FG-CNTRC-micro sandwich plate", *Steel Compos. Struct. Int. J.*, **26**(3), 273-287. http://dx.doi.org/10.12989/scs.2018.26.3.273

Kwon, D.J., Shin, P.S., Kim, J.H., DeVries, K.L. and Park, J.M. (2017), "Evaluation of optimal dispersion conditions for CNT reinforced epoxy composites using cyclic voltammetry measurements", *Adv. Compos. Mater.*, **26**(3), 219-227.

Lee, Y.I., Kim, S., Lee, K.J., Myung, N.V. and Choa, Y.H. (2013), "Inkjet printed transparent conductive films using water-dispersible single-walled carbon nanotubes treated by UV/ozone irradiation", *Thin Solid Films.*, **536**, 160-165.

Lee, S.O., Rhee, K.Y. and Park, S.J. (2015), "Influence of chemical surface treatment of basalt fibers on interlaminar shear strength and fracture toughness of epoxy-based composites", *J. Industrial. Eng. Chem.*, **32**, 153-156.

Li, J., Sham, M.L., Kim, J.K. and Marom, G. (2007), "Morphology and properties of UV/ozone treated graphite nanoplatelet/epoxy nanocomposites", *Compos. Sci. Technol.*, **67**(2), 296-305.

Li, Y., Zhang, H., Liu, Y., Wang, H., Huang, Z., Peijs, T. and Bilotti, E. (2018), "Synergistic effects of spray-coated hybrid carbon nanoparticles for enhanced electrical and thermal surface conductivity of CFRP laminates", *Compos. Part A Appl. Sci. Manuf.*, **105**, 9-18.

Liu, Y. and Wilkinson, A. (2018), "Rheological percolation behaviour and fracture properties of nanocomposites of MWCNTs and a highly crosslinked aerospace-grade epoxy resin system", *Compos. Part A Appl. Sci. Manuf.*, **105**, 97-107.

Ma, P.C., Mo, S.Y., Tang, B.Z. and Kim, J.K. (2010), "Dispersion, interfacial interaction and re-agglomeration of functionalized carbon nanotubes in epoxy composites", *Carbon*, **48**(6), 1824-1834.

Mawhinney, D.B., Naumenko, V., Kuznetsova, A., Yates, J.T., Liu, J. and Smalley, R.E. (2000), "Infrared spectral evidence for the etching of carbon nanotubes: ozone oxidation at 298 K", *J. Am. Chem. Soc.*, **122**(10), 2383-2384.

Mishra, S., Dwivedi, J., Kumar, A. and Sankararamakrishnan, N. (2016), "Removal of antimonite (Sb (III)) and antimonate (Sb (V)) using zerovalent iron decorated functionalized carbon nanotubes", *RSC Adv.*, **6**(98), 95865-95878.

Mittal, G. and Rhee, K.Y. (2018), "Chemical vapor deposition-based grafting of CNTs onto basalt fabric and their reinforcement in epoxy-based composites", *Compos. Sci. Technol.*, **165**, 84-94.

Moradi-Dastjerdi, R. and Payganeh, G. (2017), "Transient heat transfer analysis of functionally graded CNT reinforced cylinders with various boundary conditions", *Steel Compos. Struct. Int. J.*, **24**(3), 359-367.

Najafi, E., Kim, J.Y., Han, S.H. and Shin, K. (2006), "UV-ozone treatment of multi-walled carbon nanotubes for enhanced organic solvent dispersion", *Colloid. Surf. A Physicochem. Eng. Aspects.*, **284**, 373-378.

Ö ztürk, B.Ü .L.E.N.T., Arslan, F. and Ö ztürk, S.U.L.T.A.N. (2007), "Hot wear properties of ceramic and basalt fiber reinforced hybrid friction materials", *Tribol. Int.*, **40**(1), 37-48.

Owens, D.K. and Wendt, R.C. (1969), "Estimation of the surface free energy of polymers", *J. Appl. Polym. Sci.*, **13**(8), 1741-1747.

Quagliarini, E., Monni, F., Lenci, S. and Bondioli, F. (2012), "Tensile characterization of basalt fiber rods and ropes: A first contribution", *Constr. Build. Mater.*, **34**, 372-380.

Ravindran, A.R., Ladani, R.B., Wu, S., Kinloch, A.J., Wang, C.H. and Mouritz, A.P. (2018), "Multi-scale toughening of epoxy composites via electric field alignment of carbon nanofibres and short carbon fibres", *Compos. Sci. Technol.*, **167**, 115-125.

Ray, B.C. (2004), "Thermal shock on interfacial adhesion of thermally conditioned glass fiber/epoxy composites", *Mater. Lett.*, **58**(16), 2175-2177.

Ray, B.C. (2006), "Temperature effect during humid ageing on interfaces of glass and carbon fibers reinforced epoxy composites", *J. Colloid Interf. Sci.*, **298**(1), 111-117.

Ryu, S.K., Park, B.J. and Park, S.J. (1999), "XPS analysis of carbon fiber surfaces-anodized and interfacial effects in fiber–epoxy composites", *J. Colloid Interf. Sci.*, **215**(1), 167-169.

Sarasini, F., Tirillò, J., Valente, M., Valente, T., Cioffi, S., Iannace, S. and Sorrentino, L. (2013), "Effect of basalt fiber hybridization on the impact behavior under low impact velocity of glass/basalt woven fabric/epoxy resin composites", *Compos. Part A Appl. Sci. Manuf.*, **47**, 109-123.

Sham, M.L. and Kim, J.K. (2006), "Surface functionalities of multi-wall carbon nanotubes after UV/Ozone and TETA treatments", *Carbon*, **44**(4), 768-777.

Shi, X.H., Xu, Y.J., Long, J.W., Zhao, Q., Ding, X.M., Chen, L. and Wang, Y.Z. (2018), "Layer-by-layer assembled flame-retardant architecture toward high-performance carbon fiber composite", *Chem. Eng. J.*, **353**, 550-558.

Shishevan, F.A., Akbulut, H. and Mohtadi-Bonab, M.A. (2017), "Low velocity impact behavior of basalt fiber-reinforced polymer composites", *J. Mater. Eng. Perform.*, **26**(6), 2890-2900.

Shokravi, M. (2017), "Buckling of sandwich plates with FG-CNT-reinforced layers resting on orthotropic elastic medium using Reddy plate theory", *Steel Compos. Struct. Int. J.*, **23**(6), 623-631.

Sui, C., Pan, Z., Headrick, R.J., Yang, Y., Wang, C., Yuan, J. and Lou, J. (2018), "Aligned-SWCNT film laminated nanocomposites: Role of the film on mechanical and electrical properties", *Carbon*, **139**, 680-687.

Tahouneh, V. (2018), "3-D vibration analysis of FG-MWCNTs/phenolic sandwich sectorial plates", *Steel Compos. Struct. Int., J*, **26**(5), 649-662.

Tang, L.C., Zhang, H., Han, J.H., Wu, X.P. and Zhang, Z. (2011), "Fracture mechanisms of epoxy filled with ozone functionalized multi-wall carbon nanotubes", *Compos. Sci. Technol.*, **72**(1), 7-13.

Wang, G., Wei, X., Tanaka, T. and Kataura, H. (2018), "Facile synthesis of guar gum gel for the separation of metallic and semiconducting single-wall carbon nanotubes", *Carbon*, **129**, 745-749.

Wong, E.W., Sheehan, P.E. and Lieber, C.M. (1997), "Nanobeam mechanics: elasticity, strength, and toughness of nanorods and nanotubes", *Science*, **277**(5334), 1971-1975.

Xu, Z., Yue, M., Chen, L., Zhou, B., Shan, M., Niu, J. and Qian, X. (2014), "A facile preparation of edge etching, porous and highly reactive graphene nanosheets via ozone treatment at a moderate temperature", *Chem. Eng. J.*, **240**, 187-194.

Yim, Y.J., Rhee, K.Y. and Park, S.J. (2015), "Influence of electroless nickel-plating on fracture toughness of pitch-based carbon fibre reinforced composites", *Compos. Part B. Eng.*, **76**, 286-291.

Zhang, Y., Yu, C., Chu, P.K., Lv, F., Zhang, C., Ji, J. and Wang, H. (2012), "Mechanical and thermal properties of basalt fiber reinforced poly (butylene succinate) composites", *Mater. Chem. Phys.*, **133**(2-3), 845-849.

CC